AGU PUBLICATIONS

JGR

Journal of Geophysical Research: Space Physics

RESEARCH ARTICLE
10.1002/2016JA023836

Key Points:
- A much higher occurrence rate of weak B_s events is found than that of stronger B_s
- Many of the weak B_s events originate from regions other than ICMEs and high-speed streams
- Even weak B_s events are often geoeffective and these include substorms and disturbances of the outer radiation belt

Correspondence to:
D.-Y. Lee,
dylee@chungbuk.ac.kr

Citation:
Choi, K.-E., D.-Y. Lee, K.-C. Choi, and J. Kim (2017), Statistical properties and geoeffectiveness of southward interplanetary magnetic field with emphasis on weakly southward B_z events, *J. Geophys. Res. Space Physics*, *122*, doi:10.1002/2016JA023836.

Received 23 DEC 2016
Accepted 10 MAY 2017
Accepted article online 11 MAY 2017

Statistical properties and geoeffectiveness of southward interplanetary magnetic field with emphasis on weakly southward B_z events

Kyung-Eun Choi[1], Dae-Young Lee[1], Kyu-Cheol Choi[2], and Jaehun Kim[3]

[1]Department of Astronomy and Space Science, Chungbuk National University, Cheongju, South Korea, [2]Research Institute, SELab, Inc., Seoul, South Korea, [3]Korean Space Weather Center, National Radio Research Agency, Jeju, South Korea

Abstract In this work we analyze the statistical properties and geoeffectiveness of southward interplanetary magnetic field (IMF) B_z (B_s) events measured near the Earth from 1996 to 2015. We classify the B_s events into six contrasting classes according to the duration and intensity of B_s: two subclasses of long-lasting major intensity, two subclasses of long-lasting weak intensity, and two subclasses of short-lasting weak intensity. We find the following results. (1) The occurrence rate of B_s events is lowest for the long-lasting major-intensity B_s classes and increases toward shorter-lasting and weaker-intensity B_s classes. (2) Many of the B_s events in nearly all classes are associated with regions other than interplanetary coronal mass ejections and coronal hole high-speed streams. (3) Alfvén waves account for a significant fraction of the B_s events (e.g., ~60% for the short-lasting and weak-intensity B_s classes). (4) There are clear differences in solar cycle dependence of B_s events among the different B_s classes. (5) Even either the long-lasting or short-lasting weak-intensity class B_s events can often be geoeffective by triggering substorms of weak-to-medium intensity and by enhancing geosynchronous relativistic electron fluxes. In conclusion, we emphasize that even the weakly (in terms of either intensity or duration) southward IMF B_z should be considered significant from the viewpoint of their high occurrence rate and their geoeffectiveness compared to those of long-lasting major intensity.

1. Introduction

It is well known that geomagnetic storms are caused by a strong southward interplanetary magnetic field (IMF) B_z. There have been many studies, indicating that the intensity of a geomagnetic storm is closely related to the magnitude and duration of southward IMF B_z. For example, *Gonzalez et al.* [1994] found that long southward B_z (>3 h) almost always causes a strong geomagnetic storm (minimum $Dst < -100$ nT). *Wu and Lepping* [2002] examined 135 magnetic clouds and found that the *Dst* index correlates well with both the IMF B_z component and the solar wind electric field, $V_{sw}B_s$. They further found that the correlation coefficient for *Dst* versus IMF B_z increases dramatically when the solar wind speed exceeds 600 km/s. *Gopalswamy et al.* [2008] also reported that two thirds of their 99 magnetic clouds are geoeffective; the *Dst* index was highly correlated with the solar wind speed and the magnetic field in the magnetic clouds as well as their product.

Substorm occurrence is also related to IMF conditions. However, the relation is rather complex [*Kamide*, 2001]. While mostly it is the southward IMF B_z that is required for preconditioning prior to substorm occurrence, other situations can be also related to substorm occurrence such as northward turning of IMF B_z [e.g., *Lyons et al.*, 1997] and even continuously northward IMF B_z conditions [*Lee et al.*, 2010]. In fact, it is known that Alfvénic IMF fluctuations during coronal hole high-speed streams [*Tsurutani and Gonzalez*, 1987], involving continuous turning of IMF B_z between northward and southward directions, lead to repetitive substorms [*Lee et al.*, 2006; *H.-J. Kim et al.*, 2008]. In addition, storms usually accompany substorms, namely, the so-called "storm time substorms" [*Kamide*, 2001], as a southward IMF B_z is a common factor to occurrence of both storms and substorms. A short review of recent advances in substorm research can be found in *Sergeev et al.* [2012, and reference therein].

It is well known that relativistic electron fluxes in the outer radiation belt often change significantly in response to the major solar activity such as interplanetary coronal mass ejections (ICMEs) and coronal hole high-speed streams [e.g., *Reeves et al.*, 2003; *Lyons et al.*, 2005], which accompany southward IMF B_z

conditions. The radiation belt dynamics can be affected in a sensitive way by storms and substorms, which produce energetic particles and plasma waves of various kinds (see a review by *Friedel et al.* [2002]). From a practical viewpoint, understanding the relativistic electron dynamics is critical as they can cause fatal failures of spacecraft operations through "deep dielectric charging" [*Gussenhoven et al.*, 1991; *Baker et al.*, 1994]. *Baker* [2000] reported that two spacecraft failures in 1998 occurred at the time when the >2 MeV geosynchronous electron flux level reached ~2×10^3/cm^2/s/sr.

Thus, it is of critical importance to understand the characteristics of southward IMF B_z conditions with different origins and the relative importance of their geoeffectiveness.

ICMEs and coronal hole high-speed streams are two types of major solar activity, which provides southward IMF B_z conditions [*Klein and Burlaga*, 1982; *Wilson*, 1987; *Lindsay et al.*, 1995; *Tsurutani et al.*, 2006; *Gopalswamy,* 2016]. Therefore, many previous studies of the geoeffectiveness of southward IMF B_z have concentrated on them. However, it is not unreasonable to consider the possibility that some southward IMF B_z conditions are not related to ICMEs and coronal hole high-speed streams. In fact, *Zhang and Moldwin* [2014] suggested that a quarter of the strongly southward IMF B_z events ($t > 6$ h, $B_z < -10$ nT) was not related to any well-defined solar wind structure. Also, *Zhang et al.* [2014] analyzed southward IMF B_z events defined by $t > 1$ h and $B_z < -5$ nT that were unrelated with any well-defined solar wind structure at 1 AU. They found that one third of the southward IMF events show the features of Alfvén waves and more than half of them originate from the slow solar wind. Motivated by these recent works [*Zhang and Moldwin,* 2014; *Zhang et al.*, 2014], we revisit the similar problem of the statistical features and geoeffectiveness of southward IMF B_z events measured near the Earth. In contrast to the previous works, we pay a special attention to the extent to which weakly southward IMF B_z events are significant in terms of occurrence rate and geoeffectiveness compared to strongly southward IMF B_z events.

For this work, we define six classes of southward IMF B_z events according to their intensity and duration. We derive the general statistical features of the six classes. In addition, our analysis includes determination of the extent to which the identified southward B_z events of each class are associated with ICMEs, coronal hole high-speed streams, and Alfvén waves. Finally, we check the geoeffectiveness of each of the different classes of southward B_z events.

The paper is organized as follows. In section 2, we describe the data used for the analysis and the methodology employed in this work. In section 3, we present the analysis results. Lastly, a summary and discussion are given in section 4.

2. Data and Methodology

To identify a southward IMF B_z event, B_s, we used the IMF data for 20 years from 1996 to 2015 which are available on NASA's OMNI website, http://omniweb.gsfc.nasa.gov//. We used the B_z data in the Geocentric Solar Ecliptic (GSE) coordinate system and at 5 min time resolution. It is B_z defined in the geocentric solar magnetospheric (GSM) coordinate system that can describe more suitably the interaction between IMF and the major magnetospheric phenomena such as storms and substorms. However, to avoid additional issues such as the diurnal variation of B_z in GSM, we use B_z in GSE for this study.

For this work, we determine a "B_s event" by requiring that IMF B_z is negative continuously for a certain time interval based on the 5 min time resolution data. We identified six groups of B_s events according to different durations and intensity of southward B_z: Specifically, they are "Long-Strong B_s," "Long-Medium B_s," "Long-Weak $B_s \geq 3$ h," "Long-Weak $B_s \geq 1$ h," "Short-Weak B_s 1," and "Short-Weak B_s 2." The naming of each B_s event reflects duration and intensity of southward B_z: In this aspect, the six classes are well distinguished. The specific conditions for definition of each class are summarized in the second and third columns of Table 1. Long-Strong B_s class is defined by the condition that B_z remains southward for 3 h or longer during which its minimum value is -10 nT or less. Long-Medium B_s class is defined similarly except that the minimum B_z is relaxed to be -5 nT or less. Note that the Long-Medium B_s class automatically includes the Long-Strong B_s class. We compare these two classes with an intention to see if the stronger B_s condition can make any major difference. The next two classes, Long-Weak $B_s \geq 3$ h and Long-Weak $B_s \geq 1$ h, reflect southward B_z events with weaker intensity having B_z minimum between 0 and -5 nT, but with different durations of southward

Table 1. The Criteria and Basic Statistics of B_s Event Classes[a]

	Criteria of B_z		Statistics	
B_s Classes	Duration	Minimum	Event Numbers	Summed Duration[a]
Long-Strong B_s	≥3 h	≤−10 nT	397	139 days (2%)
Long-Medium B_s	≥3 h	≤−5 nT	2,240	616 days (8%)
Long-Weak $B_s \geq 3$ h	≥3 h	0 to −5 nT	3,680	780 days (11%)
Long-Weak $B_s \geq 1$ h	≥1 h	0 to −5 nT	15,663	1626 days (22%)
Short-Weak B_s 1	30 min–60 min	0 to −5 nT	15,800	513 days (7%)
Short-Weak B_s 2	15 min–45 min	0 to −5 nT	28,671	613 days (8%)

[a]The value in parenthesis is the percentage duration of each class during the 20 year measurement period.

interval, ≥3 h and ≥1 h, respectively. To be practical with these long lasting durations, i.e., ≥3 h and ≥1 h, we allowed a very brief deviation of B_z from the southward direction to northward direction as long as this occurs only at a single data point of 5 min time resolution. Note that the Long-Weak $B_s \geq 1$ h class automatically includes the Long-Weak $B_s \geq 3$ h class. We test these classes with an intention to see if the longer-lasting B_s condition can make any major difference since we see no definite reason for having to select a specific duration when defining a "long-lasting" event. The last two classes, Short-Weak B_s 1 and Short-Weak B_s 2, represent southward B_z events with weak intensity (B_z minimum between 0 and −5 nT) and short durations, 30 min–60 min and 15 min–45 min, respectively. The durations of these two Short-Weak classes overlap to some extent, and we have deliberately chosen these two durations with an intention to test any sensitivity of the statistical results to small but different durations. Figure 1 shows some examples of B_s event classes identified for an interval in 2015. The purpose with the six-class classification is to compare B_s events of different intensity and duration from perspectives of their origin and geoeffectiveness.

Our examination of the origin of the six classes of B_s checked occurrences of the major solar activity, namely, interplanetary coronal mass ejections and coronal hole high-speed streams, as well as for the existence of Alfvén waves in the solar wind. Also, we checked the dependence of each class on the sunspot cycle. In addition, we compared the six classes in terms of accompanying solar wind variables such as the solar wind speed, IMF magnitude, solar wind density, and temperature.

Our examination of the geoeffectiveness by B_s of the six classes focused on three major phenomena, namely, the occurrence of substorms (monitored by *AL* index), the occurrence of magnetic storms (based on *SYM-H* index), and the outer radiation belt disturbance (using >2 MeV electron fluxes at geosynchronous orbit).

3. Statistical Results

3.1. The Basic Statistics of B_s Events

Table 1 shows a summary of the definition and statistics for the six classes of B_s events, which we obtained based on the methods described in section 2. The criteria for each class are summarized in the second and third columns in Table 1. The fourth column shows the number of independent events in each B_s class. The last column refers to the summed duration over all of the B_s events for each class, and the corresponding

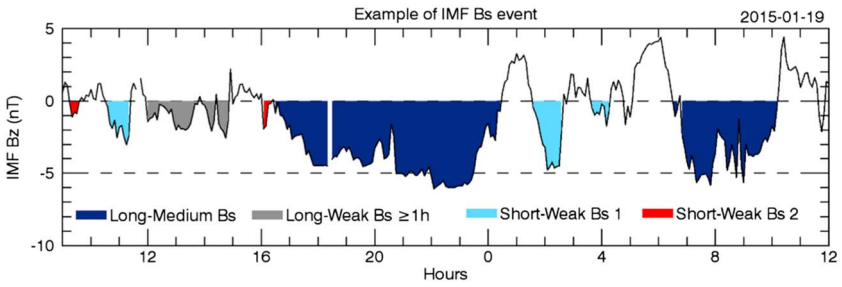

Figure 1. An example of IMF B_s events. Four classes of B_s events out of the six classes in Table 1 are identified. The two short intervals of $B_z < 0$ at ~05:00 UT and ~11:30 UT on 19 January 2015 are shorter than 15 min and do not satisfy the selection criteria in Table 1, and thus, they are not identified as an event here.

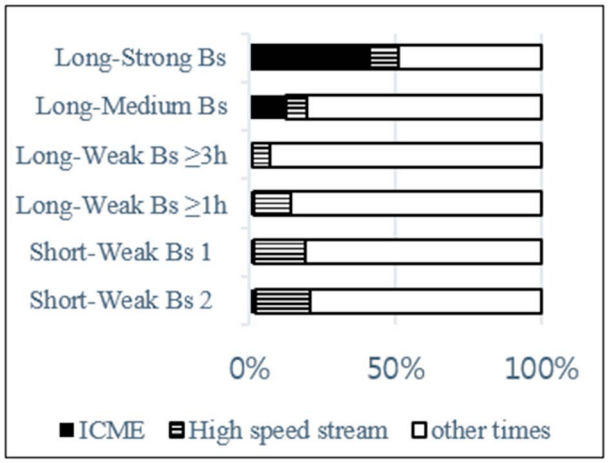

Figure 2. The solar events contribution to B_s classes.

percentage rate (shown in parenthesis) out of the total 20 year time interval studied. Note that the summed durations in total correspond to <45% of 20 years (It should be recalled that Long-Medium class automatically includes Long-Strong class, Long-Weak $B_s \geq 1$ h class includes Long-Weak $B_s \geq 3$ h class, and there is some overlap between the two Short-Weak classes). There is the remaining >55% interval which consists of the southward B_z conditions that did not satisfy our selection criteria and of course the locations where the IMF B_z was northward. Not surprisingly, the number of B_s events is smallest for Long-Strong B_s class and rapidly increases toward the classes of weaker intensity and shorter interval (from top to bottom rows). The statistics is somewhat different in terms of the summed durations. It shows that the summed durations are short for the Long-Strong and Long-Medium classes and increase for the Long-Weak B_s class ≥ 1 h being the longest duration among the six classes. The total durations of the two Short-Weak B_s classes are shorter mainly due to their definitions requiring short durations, although the occurrence percentage rates of their independent event classes are two of the highest.

3.2. The Origin of Each Class of B_s Events

We studied the origin of B_s events to determine the possible differences among the different B_s classes. First, for each B_s event, we checked their association with ICMEs and coronal hole high-speed streams. For determining the occurrence of ICME events, we relied mostly on the sharp changes in the IMF and the proton temperature and density as demonstrated in *Kamide et al.* [1998], *Cane and Richardson* [2003], and *Richardson and Cane* [2010] as well as on the website, http://www.srl.caltech.edu/ACE/ASC/DATA/level3/icmetable2.htm. For determining the occurrence of the coronal hole high-speed streams, we used a criterion of the solar wind speed being over 500 km/s continuously for 2 days or longer with a peak speed of 600 km/s or larger. The selected events were all confirmed by visual inspection for consistency with the generally known features of coronal hole high-speed streams including the existence of the compressed corotaing interaction region followed by long-lasting Alfvénic fluctuating main body of the high-speed streams, and a repetitive occurrence every ~27 days [e.g., *Rosenberg and Coleman*, 1980; *Kamide et al.*, 1998].

The results are presented in Figure 2, which shows that out of the Long-Strong B_s class events, ~41% and ~10% are associated with ICMEs and coronal hole high-speed streams, respectively. For the Long-Medium B_s class events, the association with ICMEs and coronal hole high-speed streams becomes less, being ~12% and ~8%, respectively. In contrast, the association with ICMEs becomes negligible for the other four B_s classes, which is not surprising because magnetic fields in ICMEs generally represent a significant enhancement over the background IMF. Instead, the association with coronal hole high-speed streams becomes greater for the Short-Weak B_s classes.

However, it should be emphasized that the majority of B_s events are associated with "other times," ranging ~50% for Long-Strong class to ~79% for Short-Weak 2 class. This implies a possible origin of B_s due to reasons in the solar wind other than the periods of major solar activity. Specifically, the "other times" in Figure 2 must primarily be locations where the solar wind conditions have not well defined ICMEs and high-speed streams. However, they could partly include the interplanetary small-scale magnetic flux ropes (ISMFR) [*Moldwin et al.*, 2000; *Feng et al.*, 2008, 2010; *Zhang et al.*, 2013], and the conditions associated with shocks and discontinuities [*Burlaga*, 1968, 1970; *Tsurutani and Ho*, 1999]. In the present work, we have not identified ISMFRs, shocks, and discontinuities, which were, however, distinguished in the previous work by *Zhang and Moldwin* [2014]. In addition, we caution that in determining the association of B_s with ICMEs, we have not included the sheath region ahead of the ICME body. Thus, the "other times" includes the B_s events found in the sheath region

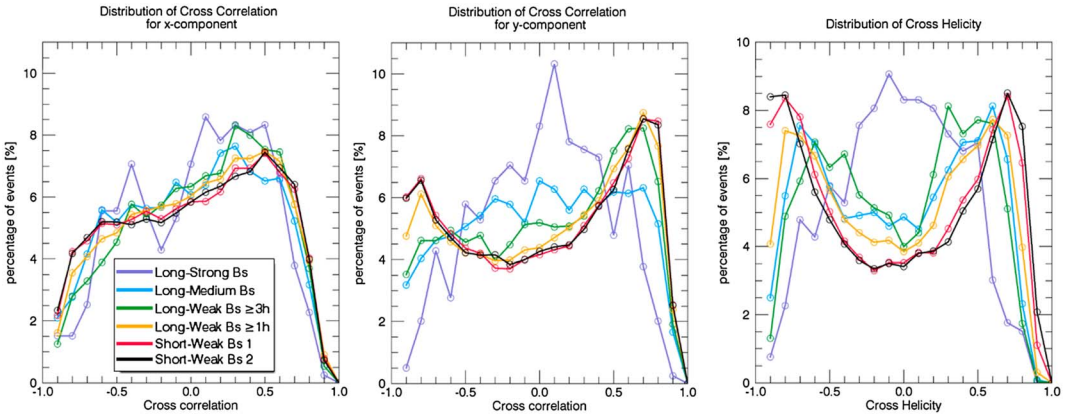

Figure 3. Distribution of cross correlations and cross helicity for the six classes of B_s events. (left and middle) Cross correlations refer to those between B_x and V_x and between B_y and V_y, respectively. (right) Cross helicity represents a degree of "Alfvénicity" based on the definition shown in the text.

ahead of ICMEs, but the number of such B_s events is small (<10% of other times for the Long-Strong B_s class events to which the ICME contribution is largest).

To examine the possible origins of B_s events from other than major solar activity, we checked for the existence of Alfvén waves in association with B_s events. We have done this by estimating the cross correlations between the magnetic field and solar wind velocity components [*Belcher and Davis*, 1971; *Tsurutani and Ho*, 1999]. Specifically, we have estimated them between B_x and V_x, and between B_y and V_y. For further confirmation, we have also tested the cross helicity σ_c as in *Riley et al.* [1996], which is defined by $\sigma_c = 2\delta V \cdot \delta V_A/(\delta V^2 + \delta V_A{}^2)$, where δV and δV_A mean the solar wind velocity fluctuations and the Alfvén wave velocity fluctuations, respectively [*Matthaeus and Goldstein*, 1982]. When the magnitude of σ_c is close to unity, the fluctuations are considered to be Alfvénic. The computed results are shown in Figure 3. For Long-Strong B_s class events (violet lines), the distributions of the correlation coefficients and the cross helicity tend to peak around zero. In contrast, the distributions for the Long-Weak and Short-Weak B_s classes show the tendency for the peak correlations (in particular in y component) and helicity to occur at higher values. This tendency is most prominent for the Short-Weak B_s 1 and 2 class events (black and red lines), the peaks occurring at ~0.5 and ~0.7 for the *x* and *y* component correlation coefficients, respectively, and ~0.7 for the cross helicity. A similar tendency is also noted for the two Long-Weak classes (yellow and green lines). For the Long-Medium class, the distribution of cross helicity is similar to those of the Long-Weak and Short-Weak B_s classes, but those of cross correlations are less well distinguished.

If we choose to impose the specific requirement, simply to be practical, that the absolute values of cross correlation for either *x* or *y* component are >0.5 to determine the existence of Alfvén waves, we obtain the results in Figure 4 showing the statistics of the contributions by the Alfvén waves to B_s events of each class. It is seen from Figure 4 that Alfvén wave contribution is larger when the B_s event is shorter in duration and/or weaker in intensity. In particular, for the four weak B_s classes, the Alfvén wave contribution is ~50–60%. In contrast, for the Long-Strong B_s class, the contribution is ~17%.

Here we add a short comment on the amplitude of Alfvén wave B_s in comparison with that of ICMEs. First, the average B_s values of ICMEs that were identified in the Long-Strong and Long-Medium classes are −9.7 nT and −7.6 nT, respectively. For the Alfvén waves of the same classes, the average B_s values are −9.3 nT and −3.3 nT, respectively. For the Alfvén waves of the other four weaker classes, the average B_s values range from −1.3 nT to −1.7 nT (Note that the definition of these four classes requires the B_s values range between 0 and −5 nT).

In addition, we investigated, though partially, the origin of Alfvén waves identified in Figure 4 in particular by determining the extent to which they are associated with ICMEs and coronal hole high-speed streams. The results are shown in Figure 5. The association of Alfvén waves with ICMEs and coronal hole high-speed streams is largest (~48% together) for Long-Strong B_s class, and it becomes much smaller for Long-Medium

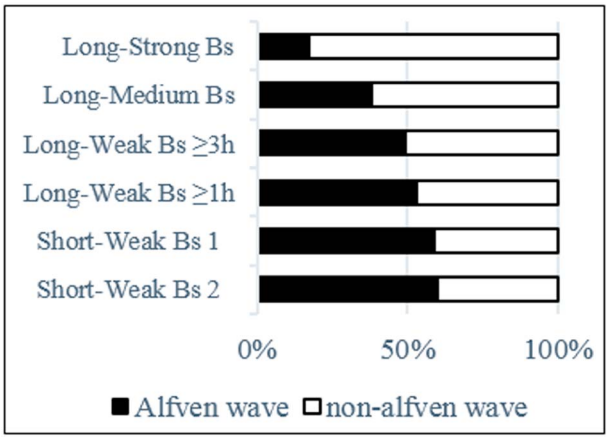

Figure 4. Alfvén wave contribution to B_s events of the six classes.

class (~18%). For the four weak B_s classes, Alfvén wave events are more associated with coronal hole high-speed streams, which is well known [e.g., *Tsurutani and Gonzalez*, 1987; *Lee et al.*, 2006]. We emphasize that more than half of the identified Alfvén events for all of the six classes are not associated with either ICMEs or coronal hole high-speed streams, further study of which is left for future work.

In Table 2, we present the Alfvén wave results of Figures 4 and 5 in a different way in combination with Figure 2. Specifically, the second column in Table 2 shows the fraction of Alfvén waves out of the B_s events that are associated with ICMEs/high-speed streams in Figure 2. Likewise, the third column in Table 2 refers to the fraction of Alfvén waves out of the B_s events that are associated with other times in Figure 2. With these, we intend to determine the extent to which Alfvén waves contribute to a group of B_s events with two different origins (ICMEs/high-speed streams versus other times) and compare the results among the six B_s classes. The second column in Table 2 clearly indicates that when B_s events are found in association with ICMEs or high-speed streams, the Alfvén wave contribution is quite large, ~70%–79%, for the four Long-Weak and Short-Weak classes while it is much lower for the Long-Strong and Long-Medium classes. Recall from Figure 2 that for the four Long-Weak and Short-Weak classes, the association of B_s events with high-speed streams is dominant over that with ICMEs and the situation is roughly opposite for the Long-Strong and Long-Medium classes. The third column in Table 2 shows that the Alfvén wave contribution is still substantial when B_s events are found at times other than during the well-defined solar activity, near 50% for the four Long-Weak and Short-Weak classes but less for the Long-Strong and Long-Medium classes. As mentioned in section 1, *Zhang et al.* [2014] reported that one third of southward IMF B_z events, which are defined by $t > 1$ h and $B_z < -5$ nT and by being unrelated with any well-defined solar wind structure at 1 AU, show the features of Alfvén waves. The B_s events in our classification that are closest to, but not precisely the same as, the B_s events in *Zhang et al.* [2014] are those of Long-Medium B_s class found in times other than ICMEs/high-speed streams. The fraction of Alfvén wave contribution to this B_s class is ~39% as shown in Table 2, which is not too different from the result of *Zhang et al.* [2014].

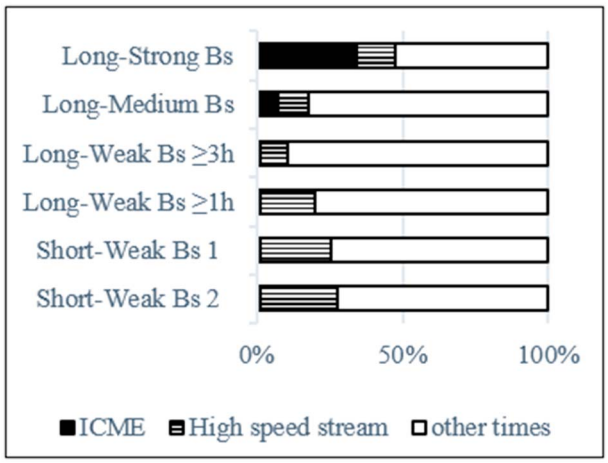

Figure 5. Origin of Alfvén waves identified in Figure 4.

We checked the solar cycle dependence of each B_s class. Figure 6 shows the results where the number of the B_s events, and the corresponding durations are shown in black and red lines, respectively. In each panel, the dashed lines refer to the contribution by the Alfvén waves. The last panel is the sunspot number. First, there are clear differences in the solar cycle dependence among the six classes. The top two panels clearly show that the number of the events and the corresponding durations of the Long-Strong and Long-Medium B_s

Table 2. Percentages of the Contributions by Alfvén Waves to B_s Events

B_s Classes	ICME/High-Speed Stream[a] (%)	Other Times[b] (%)
Long-Strong B_s	15.9	18.1
Long-Medium B_s	33.6	39.1
Long-Weak $B_s \geq 3$ h	70.8	47.3
Long-Weak $B_s \geq 1$ h	74.6	49.5
Short-Weak B_s 1	79.3	54.3
Short-Weak B_s 2	79.3	54.9

[a]Refer to the percentage of Alfvén waves out of the B_s events which are associated with ICME/high-speed streams in Figure 2.
[b]Refer to the percentage of Alfvén waves out of the B_s events which are associated with other times in Figure 2.

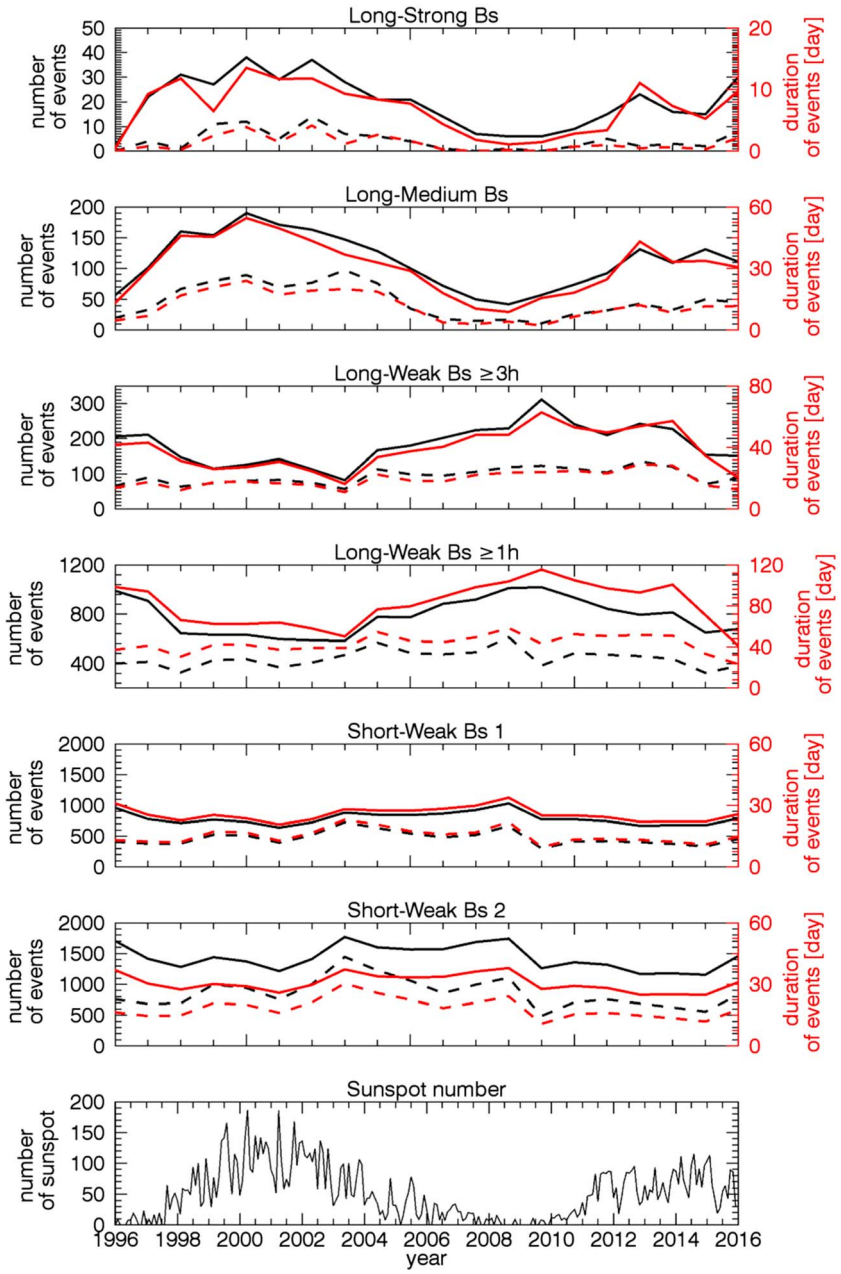

Figure 6. Yearly distribution of the number of the events (black lines) and durations (red lines) for the six B_s class events, their associated Alfvén wave contributions (dashed lines), and the sunspot cycle (seventh panel) for the 20 year period.

classes have positive correlations with the sunspot cycle. This is reasonable for the Long-Strong B_s class to which the ICME contribution is largest (~41%) as shown in Figure 2, as the number of sunspots is proportional to the number of the CME events (and thus also of the ICME events). For the Long-Medium B_s class, the ICME contribution is substantially lower (~12%) as shown in Figure 2, and thus, the positive correlation with the sunspot cycle in Figure 6 was not necessarily expected. The Alfvén wave contributions also indicate positive correlations with the sunspot cycle. On the other hand, there is a strong asymmetry between the two solar cycles, indicating that the number and duration of the B_s events (and associated Alfvén waves) of the Long-Strong and Long-Medium B_s classes are larger and longer for solar cycle 23 than for solar cycle 24. The sunspot number declined by ~40% during solar cycle 24 compared to that during solar cycle 23. *Gopalswamy et al.* [2015a, 2015b] reported that the number of halo CMEs and magnetic clouds did not decline in cycle 24. However, it should be noted that our B_s events include both those associated with ICMEs and those not associated with ICMEs as shown in Figure 2. A further examination in this aspect is worthwhile to perform in the future.

Second, the third and fourth panels of Figure 6 show the tendency that the number of the events and durations for the two Long-Weak B_s classes are in inverse proportion to the number of sunspots. This is contrary to the Long-Strong and Long-Medium classes. However, a further examination on the intercycle dependence for the two Long-Weak B_s classes is desirable in the future. On the other hand, the Alfvén wave contributions to the two Long-Weak B_s classes do not show a significant dependence on solar cycle.

Finally, Figure 6 indicates that for the two Short-Weak B_s classes, the number of B_s events and their durations as well as the Alfvén wave contributions all indicate no obvious correlation with the solar cycle except that they appear slightly enhanced during the declining phase of solar cycle 23 and near 2009. Recall the results shown in Figure 2 that the contribution to these classes is partly due to the B_s events during coronal hole high-speed streams, which is usually dominant during the declining phase of solar cycle, and also due to the B_s events that are not associated with coronal hole high-speed streams. The overall flat distribution of B_s for these classes is likely due to the larger contribution by the latter type of B_s events, although a further study of this is also necessary in the future.

3.3. Characteristics of Solar Wind Parameters During B_s Events of Each Class

For B_s events of each class, we analyzed the solar wind conditions including IMF total B, ion number density, flow speed, and proton temperature. The results are summarized in Figure 7, which shows the distributions of the four solar wind parameters averaged over each B_s event interval with the six classes distinguished by different line colors.

First, the distribution of average solar wind speed indicates that the two Short-Weak B_s classes (red and black) have higher occurrence rates for the range of V_{sw} at ~500–700 km/s than the others do. This is mostly due to coronal hole high-speed streams, which contribute to the two Short-Weak classes to some extent (as shown in Figure 2). The distribution of the IMF total B indicates striking differences between the Long-Strong (violet) and Long-Medium (blue) B_s classes and the other four weak intensity classes. This is reasonable considering that a larger magnitude of B_z contributes more to total B. This feature is similar, but less prominent, for the solar wind ion density distribution. Finally, the only notable feature in the temperature distribution is that for Long-Weak $B_s \geq 3$ h (green), the peak percentage occurs at a lower average temperature than those of the other classes. One would expect the temperature to be lower than the normal solar wind for the B_s events if they are related to ICMEs. This may be expected, but not seen in Figure 7, particularly for the Long-Strong B_s class to which the ICME contribution is largest. The discrepancy is due to the fact that the average in Figure 7 has been obtained over the entire number of B_s events, both the events found inside the ICME intervals and those found in other regions such as the higher-temperature sheath region ahead of ICMEs. We confirmed (not shown here) that when averaged over the B_s events that are related to ICMEs only (excluding the preceding sheath region), the temperature is indeed lower than that of the normal solar wind.

3.4. Geoeffectiveness in Terms of *AL*, *SYM-H*, and Geosynchronous Electron Fluxes

In order to assess the relative significance of B_s events from the viewpoint of their geoeffectiveness and compare this among the six B_s classes, we investigated the distributions of *AL*, *SYM-H*, and geosynchronous >2 MeV electron fluxes during B_s events of each class. The results are summarized in Figure 8, which

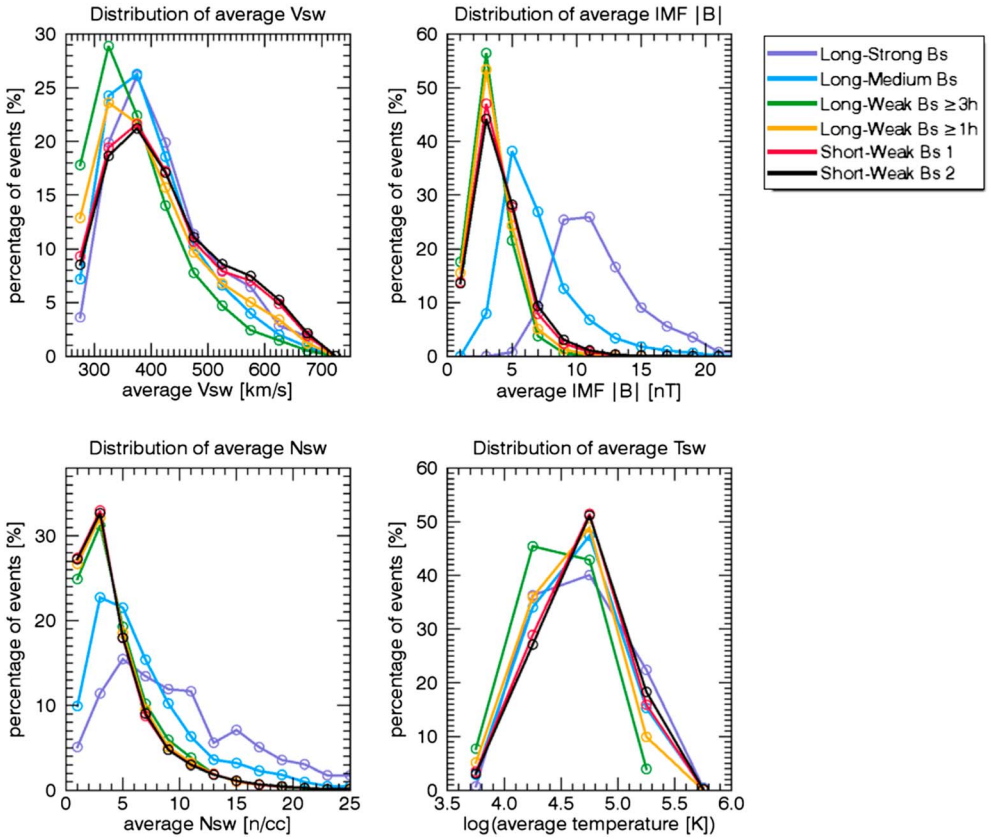

Figure 7. Distribution of solar wind parameters, solar wind speed V_{sw}, IMF B, ion number density N_{sw}, and proton temperature, as averaged over the duration of each of the B_s events.

shows clear differences among the six B_s classes. First, the left panel in Figure 8 shows the *AL* index distributions. Here we point out that *AL* is supposed to reflect the westward electrojet and it can serve as a substorm indicator when it decreases in association with a newly formed wedge current system due to substorm occurrence. At the same time, we stress that there are limitations to *AL* as a substorm indicator primarily due to the small number of magnetometer stations used (10–12 stations usually) and their uneven spatial distribution [e.g., *Gjerloev et al.*, 2004]. Nevertheless, since the substorms are characterized by multiple signatures in a complex way throughout the near-Earth magnetosphere, ionosphere, and on

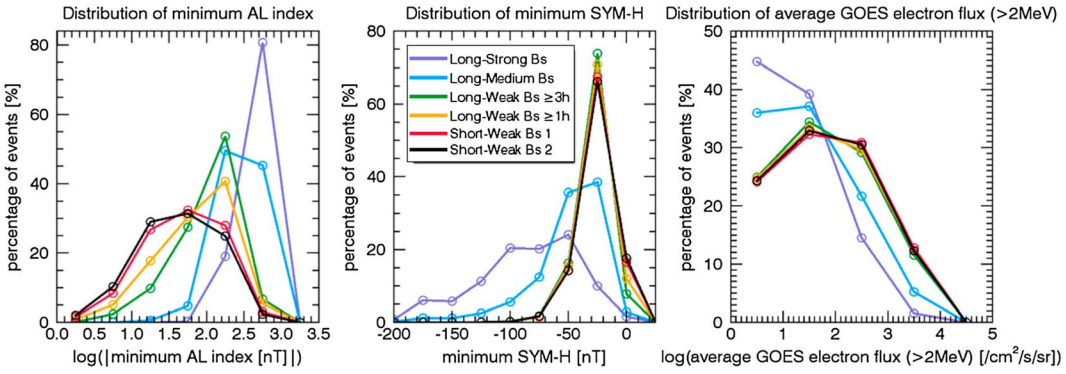

Figure 8. Distribution of *AL*, *SYM-H*, geosynchronous electron (> 2 MeV) fluxes during B_s events of each class. For *AL* and *SYM-H*, the minimum values are taken during each B_s event interval, and for the geosynchronous electron fluxes measured on GOES spacecraft, the averages are taken over each B_s event interval.

Table 3. Percentages of the Geoeffectiveness by the Bs Events of Different Classes

B_s Classes	Substorm[a] (%)	Storm[b] (%)	*e* Flux Disturbance[c] (%)
Long-Strong Bs	100	67.3	2.3
Long-Medium Bs	99.6	24.4	7.5
Long-Weak Bs ≥3h	88.8	2.3	14.9
Long-Weak Bs ≥1h	78.4	2.0	16.2
Short-Weak Bs 1	65.6	2.0	16.8
Short-Weak Bs 2	60.4	2.0	16.2

[a]Based on the criterion that $AL_{min} \leq -50$ nT [*Allen and Kroehl,* 1975].
[b]Based on the criterion that *SYM-H*$_{min} \leq -36$ nT [*Loewe and Prolss*, 1997].
[c]Based on the criterion that >2 MeV electron flux level at geosynchronous orbit ≥2×10^3/cm^2/s/sr [*Baker,* 2000; *Kim et al.*, 2006].

the ground [e.g., *Lui*, 1996; *Ohtani*, 2004; *H.-J. Kim et al.*, 2008; *Lee et al.*, 2010; *Akasofu et al.*, 2010*; Sergeev et al.*, 2012], the use of *AL* is still practical for statistical studies. In the left panel of Figure 8, it is clear that for the Long-Strong B_s class, the distribution is greatly concentrated at the highest *AL* values compared to the other B_s classes. For the weaker and shorter B_s classes, the *AL* distribution is broader and its peak shifts toward lower *AL* values. In particular, for the two Short-Weak B_s classes, the peak occurs at log |*AL*| ~1.7 corresponding to *AL* ~ −50 nT. We point out that there is no unique way to define a threshold value of *AL* beyond which a substorm is certain to occur [e.g., *Newell and Gjerloev*, 2011]. Nevertheless, if we follow the simple criterion by *Allen and Kroehl* [1975], an *AL* value below −50 nT generally represents a beginning limit for substorm occurrence. Therefore, if we adopt this criterion, more than half of the Short-Weak B_s class events are associated with substorms having *AL* = −50 nT or stronger. This implies that even a weak southward IMF B_z can often cause a substorm of weak-to-modest intensity. This finding is qualitatively consistent with the results shown in *Kamide et al.* [1977]. Table 3 summarizes the geoeffectiveness based on this criterion. Incidentally, it is well known that the onset of substorms is often preceded by a ~30 min energy buildup growth phase in the magnetotail. Our results imply that the duration of the B_s events of the two Short-Weak classes may be sufficient for setting such a substorm growth phase.

The *SYM-H* distributions for the Long-Strong and Long-Medium classes show broad distributions, indicating some fraction of B_s events occur in association with major magnetic storms. However, the peaks are present in the bin between −50 nT and −30 nT. For the other four B_s classes, the *SYM-H* distributions are much narrower with the peaks at slightly above −30 nT. *Loewe and Prolss* [1997] classified more than 1000 storms according to the intensity of *Dst* as weak (*Dst*$_{min}$ = −30 nT to −50 nT), moderate (*Dst*$_{min}$ = −50 nT to −100 nT), strong (*Dst*$_{min}$ = −100 nT to −200 nT), severe (*Dst*$_{min}$ = −200 nT to −350 nT), and great (*Dst*$_{min} < -350$ nT). The median values of *Dst*$_{min}$ are −36 nT, −68 nT, −131 nT, −254 nT, and −427 nT, respectively, for the five groups. In a more recent work on geoeffectiveness of halo coronal mass ejections by *Gopalswamy et al.* [2007], they defined that a halo CME is geoeffective if *Dst* ≤ −50 nT. They found that the median *Dst* values for backside (−41 nT), *F* limb (−58 nT) and disk halos (−97 nT) are close to the corresponding values for weak (−36 nT), moderate (−68 nT), and strong (−131 nT) storms reported by *Loewe and Prolss* [1997]. We adopt the median *Dst* value for weak storms, −36 nT, reported by *Loewe and Prolss* [1997] as the threshold for geoeffectiveness in the sense of storm occurrence. With this threshold, the percentage of the geoeffective B_s events is largest, 67.3%, for the Long-Strong B_s, becomes lower, 24.4%, for the Long-Medium B_s class, and is negligible for the other four weak classes. The statistics of the estimated geoeffectiveness is summarized in Table 3. Note that we use *SYM-H*, which is practically a high-resolution (1 min) *Dst* index and is essentially calculated by the same method as for *Dst* except for the use of different ground stations [*Iyemori*, 1990; *Wanliss and Showalter*, 2006].

Finally, the distributions of geosynchronous >2 MeV electron fluxes also show a strong contrast between the Long-Strong and Long-Medium classes and the other four weaker classes. The contrast is characterized by the feature that the electron flux enhancements occur more often for the B_s events of the four weaker classes. *Baker* [2000] reported that two spacecraft failures in 1998 occurred at the times of the >2 MeV electron flux level of ~2 × 10^3/cm^2/s/sr. *Kim et al.* [2006] used this as an approximate threshold value to define a geosynchronous relativistic electron event (GREE) in their statistical study. We are not aware of any obvious physical reasoning to define a threshold flux level, above which one can define GREEs. However, if we adopt the

criterion by *Kim et al.* [2006], ~15%–17% of the B_s events for the four weaker classes are GREEs. For the Long-Strong and Long-Medium classes, the association with the B_s events is more concentrated at low flux levels. If we continue to adopt the threshold given by *Kim et al.* [2006], only 2.3% of the B_s events of the Long-Strong class and 7.5% of the Long-Medium class correspond to GREEs, respectively (see Table 3.) This result implies that the dropout effect (loss) of the outer radiation belt electron fluxes is more important than acceleration effects (source) for the B_s conditions of the two classes, as will be discussed further in section 4. In a short summary, the occurrence rate of the geosynchronous electron disturbance due to the four weak B_s classes is larger by ~7 times than that due to the Long-Strong B_s class and by ~2 times than that due to the Long-Medium B_s class.

4. Summary and Discussion

In this paper, we identified southward directed B_s events using IMF B_z values in GSE coordinates. We associated these with solar wind parameters over 20 years measured near the Earth, derived the statistical features of these events and determined their corresponding geoeffectiveness in terms of substorms, storms, and geosynchronous relativistic electron flux disturbances. For this study, we defined six classes of B_s events according to the intensity and duration of southward B_z conditions, which are Long-Strong, Long-Medium, Long-Weak $\geq$ 3 h, Long-Weak $\geq$ 1 h, Short-Weak 1, and Short-Weak 2. We aimed to compare the characteristics of B_s events among the six classes. The main results are summarized as follows.

1. The occurrence rate of independent B_s events is lower for longer lasting and more intense B_s classes and rapidly increases toward weaker and shorter B_s classes (Table 1).
2. Our Long-Strong B_s class has the highest association (~40%) with ICMEs. Coronal hole high-speed streams are more likely associated with the weaker and shorter B_s classes. However, many of the B_s events in nearly all classes are found in regions other than ICMEs and coronal hole high-speed streams (Figure 2).
3. Alfvén waves are present for ~17% (for Long-Strong class) and ~60% (for Short-Weak class 2) of the B_s events. Many of them originate during the times other than ICMEs and coronal hole high-speed streams (Figures 4 and 5).
4. There is a clear distinction of the solar cycle dependence of B_s among the different B_s classes: while the occurrence rate of the Long-Strong and Long-Medium B_s class events is in phase with the solar cycle, the Long- Weak B_s events show negative correlation between their occurrence frequency and the solar cycle. For the Short-Weak class B_s events, the correlation is much less obvious (Figure 6).
5. The Long-Strong and Long-Medium class B_s events are mostly associated with intense *AL* and *SYM-H* conditions. In contrast, the Short-Weak class B_s events can be geoeffective in terms of triggering substorms of weak-to-medium intensity although they are unlikely to be associated with major magnetic storms. The enhancement of geosynchronous relativistic electron fluxes is more often caused by the Long-Weak and Short-Weak class B_s events than the Long-Strong and Long-Medium B_s events (Figure 8 and Table 3).

As the most important conclusion, we emphasize the potential importance of the weakly (in intensity and/or duration) southward B_z conditions for triggering substorms of weak-to-moderate intensity and for resulting in an enhancement of geosynchronous relativistic electron fluxes. This effect should not be underestimated because the weak B_s events have a much higher occurrence rate, regardless of solar cycle phase, compared to the strongly southward IMF B_z conditions which can cause the major storms and substorms. This conclusion implies that there is a necessity that the models for IMF B_z prediction [e.g., *Jackson et al.*, 2015] should cover a wide range of southward B_z conditions.

Our methodology with six classes of B_s events misses other B_s conditions that do not satisfy our selection criteria and is different from that of previous work by others [e.g., *Zhang and Moldwin*, 2014] (see the last paragraph of this section for a more detailed comparison with the work by *Zhang and Moldwin* [2014]). Nevertheless, in our classification of B_s events, the six classes are in contrast in terms of duration and/or intensity of B_s. Additionally, as a main goal, the present work demonstrates the extent to which the relatively weaker or shorter B_s conditions are significant relative to the stronger and longer B_s events from the perspectives of their occurrence rates and geoeffectiveness.

We found that some fraction of B_s is due to Alfvén waves. It is well known that a continuous Alfvén wave train is the main feature of coronal hole high-speed streams which can last several days as observed near the Earth

and cause the high-intensity long-duration continuous *AE* activity (named HILDCAA) [e.g., *Tsurutani and Gonzalez*, 1987]. However, in our study, many of the Alfvén waves are present at regions other than coronal-hole high-speed streams, a further study of which is left for a future project. Incorporation of an Alfvén wave contribution to B_s in the models for IMF B_z prediction may be worthwhile to consider. Also, while ICMEs and coronal hole streams represent large-scale structures, Alfvén waves can be of a small scale. Our study compares geoeffectiveness mainly in terms of B_s without considering the effect related to the differing spatial scales. A future study on this issue is worthwhile to perform.

We found that geosynchronous relativistic electron flux enhancements more often occur during weakly southward B_z conditions than for the more strongly southward B_z conditions which usually lead to major storms. Statistically, the high levels of geosynchronous relativistic electron flux are caused mostly by Corotating interaction region (CIR)-driven storms rather than by CME-driven storms [*Borovsky and Denton*, 2006], and high-speed streams have long been known to be a critical factor to determine the flux level of geosynchronous relativistic electrons [*Paulikas and Blake*, 1979]. Thus, the weakly southward B_z embedded in high-speed streams should be a condition favorable for geosynchronous relativistic electron flux enhancement. However, details of the net flux change involve more complex processes than the simple solar wind speed. This can be explained as follows. First, the geosynchronous electron flux level as observed at satellites is the result of delicate balance between particle source and loss [e.g., *Reeves et al.*, 2003; *Hwang et al.*, 2004; *Kim et al.*, 2006; *Lee et al.*, 2013]. In particular, the geosynchronous relativistic electron fluxes vary during the evolution of the storms. During the storm main phase the geosynchronous electrons can suffer from major flux dropouts by drift loss through the magnetopause into the solar wind leading to shrinkage of the outer radiation belt [e.g., *K. C. Kim et al.*, 2008; *Kim et al.*, 2010]. In addition, atmospheric precipitation by plasma waves can contribute to flux dropout [e.g., *Miyoshi et al.*, 2008; *Li et al.*, 2014]. Therefore, a strong B_s event, if identified during the times overlapping the storm main phase, must be associated with decrease of geosynchronous relativistic electron fluxes. During the recovery phase of storms, the geosynchronous electron flux may or may not recover to the prestorm level depending on the significance of electron acceleration relative to loss effects. Consequently, for a strong B_s event which is identified during the times overlapping the storm recovery phase, the change of geosynchronous relativistic electron fluxes may either increase or decrease. Therefore, on average the geosynchronous relativistic electron flux associated with strong B_s conditions such as during the storm times is not necessarily high. In contrast, for the weakly southward B_z conditions which do not cause a major storm but can often lead to substorms, the trapping region of the outer radiation belt electrons can expand beyond geosynchronous orbit distances and thus have no loss due to electron drift into the magnetopause. This condition favors keeping the geosynchronous electron flux maintained at a nominal (or even enhanced) level unless another major loss process exists. The substorms that occur during the weak B_s events can supply the seed particles to geosynchronous altitude which can generate plasma waves responsible for particle acceleration. Our result in Figure 8 showing the frequent occurrence of the flux enhancement for the Long-Weak and Short-Weak B_s events implies that often during these times loss processes do not dominate and instead during substorms source effects contribute to the geosynchronous electron flux to a larger extent.

Recently, *Zhang and Moldwin* [2014] performed a similar work to ours. Compared to their work, our work is distinguished in the following way. First, while they distinguished several well-defined solar wind structures in association with their B_s events such as magnetic cloud, ICMEs without MC signatures, stream-interaction regions, interplanetary small-scale magnetic flux ropes, and shocks, our groups are ICMEs without distinguishing well-defined MC from the others, and high-speed streams without excluding the corotaing interaction regions ahead of them. From the results in *Zhang and Moldwin* [2014], we note that the fractional number of the interplanetary small-scale magnetic flux ropes and shocks is small and would be included in "other times" by us. Second, there is distinction between our study and that of *Zhang and Moldwin* [2014] in categorizing B_s events. While *Zhang and Moldwin* [2014] show nine classes of B_s events in their Figure 3 and Table 1, our work employs six classes of B_s events. There is little overlap between the two studies in the categorization of B_s events. While there is no reason for having to accept some specific set of definition of B_s events against others, it is clear from comparisons between Figure 3 of *Zhang and Moldwin* [2014] and Figure 6 of ours that the solar cycle dependence of B_s events of a specific class depends on specific definition of B_s events. Most notably, we found an anticorrelation between the B_s events of the Long-Weak $B_s \geq 1$ h and

≥3 h classes and the solar cycle as shown in Figure 6 above, which was not explicitly shown in *Zhang and Moldwin* [2014]. Fourth, we have assessed the contribution by Alfvén waves for all of the six classes of B_s events, and this was not done in *Zhang and Moldwin* [2014]. Though studied in *Zhang et al.* [2014], this was done only for southward IMF B_z events defined by $t > 1$ h and $B_z < -5$ nT, unrelated to any well-defined solar wind structure. Lastly and most importantly, while *Zhang and Moldwin* [2014] examined the geoeffectiveness of various types of B_s events in relation mostly to the magnetic storms with only a limited study of substorms, we checked three aspects of geoeffectiveness, namely, magnetic storms, substorms, and geosynchronus electron flux disturbances. We further found an important contribution from weakly southward B_s events to substorms and geosynchronus electron flux disturbances. Overall, we find that our work is complementary, rather than contradictory, to the works by *Zhang and Moldwin* [2014] and *Zhang et al.* [2014], although a direct quantitative comparison cannot be made precisely due to the different methods used by these authors and us.

Acknowledgments

This work was supported by the Korean Space Weather Center of National Radio Research Agency. The work by D.-Y. Lee was also supported partly by National Research Foundation of Korea (2016M1A3A3A02017017). The solar wind data and geomagnetic indices used for this study can be obtained from OMNIWeb (http://omniweb.gsfc.nasa.gov/). The GOES electron flux data used for this study can be obtained from National Geophysical Data Center (ftp://satdat.ngdc.noaa.gov/sem/goes/data/new_avg/) NOAA. The authors are grateful to both referees for very useful comments which helped improve the manuscript.

References

Akasofu, S.-I., A. T. Y. Lui, and C.-I. Meng (2010), Importance of auroral features in the search for substorm onset processes, *J. Geophys. Res.*, *115*, A08218, doi:10.1029/2009JA014960.

Allen, J. H., and H. W. Kroehl (1975), Spatial and temporal distributions of magnetic effects of auroral electrojects as derived from *AE* indices, *J. Geophys. Res.*, *80*, 3667–3677, doi:10.1029/JA080i025p03667.

Baker, D. N. (2000), The occurrence of operational anomalies in spacecraft and their relationship to space weather, *IEEE Trans. Plasma Sci.*, *28*, 2007.

Baker, D. N., S. Kanekal, J. B. Blake, B. Klecker, and G. Rostoker (1994), Satellite anomalies linked to electron increase in the magnetosphere, *Eos Trans. AGU*, *75*, 404.

Belcher, J. W., and L. Davis Jr. (1971), Large-amplitude Alfven waves in the interplanetary medium, 2, *J. Geophy. Res.*, *76*, 3534, doi:10.1029/JA074i009p02302.

Borovsky, J. E., and M. H. Denton (2006), Differences between CME-driven storms and CIR-driven storms, *J. Geophys. Res.*, *111*, A07S08, doi:10.1029/2005JA011447.

Burlaga, L. F. (1968), Micro-scale structures in the interplanetary medium, *Sol. Phys.*, *4*, 67–92.

Burlaga, L. F. (1970), Discontinuities and shock waves in the interplanetary medium and their interaction with the magnetosphere, in *Solar-Terrestrial Physics/1970, Part II: The Interplanetary Medium*, edited by E. R. Dyer, J. G. Roederer, and A. J. Hundhausen, pp. 135–158, Springer, New York.

Cane, H. V., and I. G. Richardson (2003), Interplanetary coronal mass ejections in the near-earth solar wind during 1996–2002, *J. Geophys. Res.*, *108*(A4), 1156, doi:10.1029/2002JA009817.

Feng, H.-Q., D.-J. Wu, C.-C. Lin, J.-K. Chao, L. C. Lee, and L. H. Lyu (2008), Interplanetary small- and intermediate-sized magnetic flux ropes during 1995–2005, *J. Geophys. Res.*, *113*, A12105, doi:10.1029/2008JA013103.

Feng, H.-Q., J.-K. Chao, L. H. Lyu, and L. C. Lee (2010), The relationship between small interplanetary magnetic flux rope and the substorm expansion phase, *J. Geophys. Res.*, *115*, A09108, doi:10.1029/2009JA015191.

Friedel, R. H. W., G. D. Reeves, and T. Obara (2002), Relativistic electron dynamics in the inner magnetosphere—A review, *J. Atmos. Sol. Terr. Phys.*, *64*, 265–282.

Gjerloev, J. W., R. A. Hoffman, M. M. Friel, L. A. Frank, and J. B. Sigwarth (2004), Substorm behavior of the auroral electroject indices, *Ann. Geophys.*, *22*, 2135–2149.

Gonzalez, W. D., J. A. Joselyn, Y. Kamide, H. W. Kroehl, G. Rostoker, B. T. Tsurutani, and V. M. Vasyliunas (1994), What is a geomagnetic storm?, *J. Geophys. Res.*, *99*, 5771–5792, doi:10.1029/93JA02867.

Gopalswamy, N. (2016), History and development of coronal mass ejections as a key player in solar terrestrial relationship, *Geosci. Lett.*, *3*, 8–25, doi:10.1186/s40562-016-0039-2.

Gopalswamy, N., S. Akiyama, S. Yashiro, G. Michalek, and R. P. Lepping (2008), Solar sources and geospace consequences of interplanetary magnetic clouds observed during solar cycle 23, *J. Atmos. Sol. Terr. Phys.*, *70*, 245–253.

Gopalswamy, N., S. Yashiro, and S. Akiyama (2007), Geoeffectiveness of halo coronal mass ejections, *J. Geophys. Res.*, *112*, A06112, doi:10.1029/2006JA012149.

Gopalswamy, N., S. Yashiro, H. Xie, S. Akiyama, and P. Mäkelä (2015a), Properties and geoeffectiveness of magnetic clouds during solar cycles 23 and 24, *J. Geophys. Res. Space Physics*, *120*, 9221–9245, doi:10.1002/2015JA021446.

Gopalswamy, N., H. Xie, S. Akiyama, P. Mäkelä, S. Yashiro, and G. Michalek (2015b), The peculiar behavior of halo coronal mass ejections in solar cycle 24, *Astrophys. J.*, *804*, L23.

Gussenhoven, M. S., E. G. Mullen, D. H. Brautigam, E. Holeman, and C. Jordan (1991), Preliminary comparison of dose measurements on CRRES to NASA model predictions, *IEEE Trans. Nucl. Sci.*, *38*, 1655.

Hwang, J., K. W. Min, E. Lee, C. Lee, and D. Y. Lee (2004), A case study to determine the relationship of relativistic electron events to substorm injections and ULF power, *Geophys. Res. Lett.*, *31*, L23801, doi:10.1029/2004GL021544.

Iyemori, T. (1990), Storm-time magnetospheric currents inferred from midlatitude geomagnetic field variations, *J. Geomagn. Geoelectr.*, *42*, 1249.

Jackson, B. V., P. P. Hick, A. Buffington, H.-S. Yu, M. M. Bisi, M. Tokumaru, and X. Zhao (2015), A determination of the north-south heliospheric magnetic field component from inner corona closed-loop propagation, *Astrophys. J. Lett.*, *803*, L1, doi:10.1088/2041-8205/803/1/L1.

Kamide, Y. (2001), Interplanetary and magnetospheric electric fields during geomagnetic storms: What is more important, steady-state fields or fluctuating fields?, *J. Atmos. Sol. Terr. Phys.*, *63*, 413–420.

Kamide, Y., P. D. Perreault, D.-I. Akasofu, and J. D. Winningham (1977), Dependence of substorm occurrence probability on the interplanetary magnetic field and on the size of the auroral oval, *J. Geophys. Res.*, *82*, 5521–5528, doi:10.1029/JA082i035p05521.

Kamide, Y., et al. (1998), Current understanding of magnetic storms: Storm-substorm relationship, *J. Geophys. Res.*, *103*, 17,705–17,728, doi:10.1029/98JA01426.

Kim, H.-J., K. C. Kim, D.-Y. Lee, and G. Rostoker (2006), Origin of geosynchronous relativistic electron events, *J. Geophys. Res.*, *111*, A03208, doi:10.1029/2005JA011469.

Kim, H.-J., D.-Y. Lee, and L. R. Lyons (2008), Are repetitive particle injections during high-speed solar wind streams classic substorms?, *J. Geophys. Res.*, *113*, A08205, doi:10.1029/2007JA012847.
Kim, K. C., D.-Y. Lee, H.-J. Kim, L. R. Lyons, E. S. Lee, M. K. Öztürk, and C. R. Choi (2008), Numerical calculations of relativistic electron drift loss effect, *J. Geophys. Res.*, *113*, A09212, doi:10.1029/2007JA013011.
Kim, K. C., D.-Y. Lee, H.-J. Kim, E. S. Lee, and C. R. Choi (2010), Numerical estimates of drift loss and Dst effect for outer radiation belt relativistic electrons with arbitrary pitch angle, *J. Geophys. Res.*, *115*, A03208, doi:10.1029/2009JA014523.
Klein, L. W., and L. F. Burlaga (1982), Interplanetary magnetic clouds at 1 AU, *J. Geophys. Res.*, *87*, 613–624, doi:10.1029/JA087iA02p00613.
Lee, D.-Y., et al. (2006), Repetitive substorms caused by Alfvénic waves of the interplanetary magnetic field during highspeed solar wind streams, *J. Geophys. Res.*, *111*, A12214, doi:10.1029/2006JA011685.
Lee, D.-Y., K.-C. Choi, S. Ohtani, J. H. Lee, K. C. Kim, K. S. Park, and K.-H. Kim (2010), Can intense substorms occur under northward IMF conditions?, *J. Geophys. Res.*, *115*, A01211, doi:10.1029/2009JA014480.
Lee, D.-Y., D.-K. Shin, J.-H. Kim, J.-H. Cho, K.-C. Kim, J. A. Hwang, D. L. Turner, T. K. Kim, and M.-Y. Park (2013), Long-term loss and re-formation of the outer radiation belt, *J. Geophys. Res. Space Physics*, *118*, 3297–3313, doi:10.1002/jgra.50357.
Li, Z., et al. (2014), Investigation of EMIC wave scattering as the cause for the BARREL 17 January 2013 relativistic electron precipitation event: A quantitative comparison of simulation with observations, *Geophys. Res. Lett.*, *41*, 8722–8729, doi:10.1002/2014GL062273.
Lindsay, G. M., C. T. Russell, and J. G. Luhmann (1995), Coronal mass ejection and stream interaction region characteristic and their potential geomagnetic effectiveness, *J. Geophys. Res.*, *10*, 16,999–17,013, doi:10.1029/95JA00525.
Loewe, C. A., and G. W. Prolss (1997), Classification and mean behavior of magnetic storms, *J. Geophys. Res.*, *102*, 14,209–14,213, doi:10.1029/96JA04020.
Lui, A. T. Y. (1996), Current disruption in the Earth's magnetosphere: Observations and models, *J. Geophys. Res.*, *101*, 13,067–13,088, doi:10.1029/96JA00079.
Lyons, L. R., G. T. Blanchard, J. C. Samson, R. P. Lepping, T. Yamamoto, and T. Moretto (1997), Coordinated observations demonstrating external substorm triggering, *J. Geophys. Res.*, *102*, 27,039–27,052, doi:10.1029/97JA02639.
Lyons, L. R., D.-Y. Lee, R. M. Thorne, R. B. Horne, and A. J. Smith (2005), Solar wind-magnetosphere coupling leading to relativistic electron energization during high-speed streams, *J. Geophys. Res.*, *110*, A11202, doi:10.1029/2005JA011254.
Matthaeus, W. H., and M. L. Goldstein (1982), Measurements of the rugged invariants of magnetohydrodynamic turbulence in the solar wind, *J. Geophys. Res.*, *87*, 6011, doi:10.1029/JA087iA08p06011.
Miyoshi, Y., K. Sakaguchi, K. Shiokawa, D. Evans, J. Albert, M. Connors, and V. Jordanova (2008), Precipitation of radiation belt electrons by EMIC waves, observed from ground and space, *Geophys. Res. Lett.*, *35*, L23101, doi:10.1029/2008GL035727.
Moldwin, M. B., S. Ford, R. Lepping, J. Slavin, and A. Szabo (2000), Small-scale magnetic flux ropes in the solar wind, *Geophys. Res. Lett.*, *27*, 57–60, doi:10.1029/1999GL010724.
Newell, P. T., and J. W. Gjerloev (2011), Evaluation of SuperMAG auroral electrojet indices as indicators of substorms and auroral power, *J. Geophys. Res.*, *116*, A12211, doi:10.1029/2011JA016779.
Ohtani, S. (2004), Flow bursts in the plasma sheet and auroral substorm onset: Observational constraints on connection between midtail and near-Earth substorm processes, *Space Sci. Rev.*, *113*, 77–96.
Paulikas, G. A., and J. B. Blake (1979), Effects of the solar wind on magnetospheric dynamics: Energetic electrons at the synchronous orbit, in *Quantitative Modeling of the Magnetospheric Processes*, *Geophys. Monogr. Ser.*, edited by W. Olson, pp. 180–202, AGU, Washington, D. C., doi:10.1029/GM021p0180.
Reeves, G. D., K. L. McAdams, R. H. W. Friedel, and T. P. O'Brien (2003), Acceleration and loss of relativistic electrons during geomagnetic storms, *Geophys. Res. Lett.*, *30*(10), 1529, doi:10.1029/2002GL016513.
Richardson, I. G., and H. V. Cane (2010), Near-Earth interplanetary coronal mass ejections during solar cycle 23 (1996–2009): Catalog and summary of properties, *Sol. Phys.*, *264*, 189, doi:10.1007/s11207-010-9568-6.
Riley, P., C. P. Sonett, B. T. Tsurutani, A. Balogh, R. J. Forsyth, and G. W. Hoogeveen (1996), Properties of arc-polarized Alfvén waves in the ecliptic plane: Ulysses observations, *J. Geophys. Res.*, *101*, 19,987–19,993, doi:10.1029/96JA01743.
Rosenberg, R. L., and J. P. J. Coleman (1980), Solar cycle-dependent north-south field configurations observed in solar wind interaction regions, *J. Geophys. Res.*, *85*, 3021–3032, doi:10.1029/JA085iA06p03021.
Sergeev, V. A., V. Angelopoulos, and R. Nakamura (2012), Recent advances in understanding substorm dynamics, *Geophys. Res. Lett.*, *39*, L05101, doi:10.1029/2012GL050859.
Tsurutani, B. T., and W. D. Gonzalez (1987), The cause of high intensity long-duration continuous *AE* activity (HILDCAAs): Interplanetary Alfven wave trains, *Planet. Space Sci.*, *35*, 405–412.
Tsurutani, B. T., and C. M. Ho (1999), A review of discontinuities and Alfvén waves in interplanetary space: ULYSSES results, *Rev. Geophys.*, *37*, 517–541, doi:10.1029/1999RG900010.
Tsurutani, B. T., et al. (2006), Corotating solar wind streams and recurrent geomagnetic activity: A review, *J. Geophys. Res.*, *111*, A07S01, doi:10.1029/2005JA011273.
Wanliss, J. A., and K. M. Showalter (2006), High-resolution global storm index: *Dst* versus SYM-H, *J. Geophys. Res.*, *111*, A02202, doi:10.1029/2005JA011034.
Wilson, R. M. (1987), Geomagnetic response to magnetic clouds, *Planet. Space Sci.*, *35*, 329–335.
Wu, C.-C., and R. P. Lepping (2002), Effect of solar wind velocity on magnetic cloud-associated magnetic storm intensity, *J. Geophys. Res.*, *107*(A11), 1346, doi:10.1029/2002JA009396.
Zhang, X.-Y., and M. B. Moldwin (2014), The source, statistical properties, and geoeffectiveness of long-duration southward interplanetary magnetic field intervals, *J. Geophys. Res. Space Physics*, *119*, 658–669, doi:10.1002/2013JA018937.
Zhang, X.-Y., M. B. Moldwin, and M. Cartwright (2013), The geo-effectiveness of interplanetary small-scale magnetic flux ropes, *J. Atmos. Sol. Terr. Phys.*, *95-96*, 1–14.
Zhang, X.-Y., M. B. Moldwin, J. T. Steinberg, and R. M. Skoug (2014), Alfven waves as a possible source of long-duration, large-amplitude, and geoeffective southward IMF, *J. Geophys. Res. Space Physics*, *119*, 3259–3266, doi:10.1002/2013JA019623.